

Spectroscopic Properties of MgH₂, MgD₂, and MgHD Calculated from a New *ab Initio* Potential Energy Surface

Hui Li* and Robert J. Le Roy

Guelph-Waterloo Centre for Graduate Work in Chemistry and Biochemistry, University of Waterloo, Waterloo, Ontario N2L 3G1, Canada

Received: March 30, 2007; In Final Form: May 8, 2007

A three-dimensional potential energy surface for the ground electronic state of MgH₂ has been constructed from 9030 symmetry-unique *ab initio* points calculated using the icMRCI+Q method with aug-cc-pVnZ basis sets for $n = 3, 4,$ and $5,$ with core-electron correlation calculated at the MR-ACPF level of theory using cc-pCVnZ basis sets, with both calculations being extrapolated to the complete basis set limit. Calculated spectroscopic constants of MgH₂ and MgD₂ are in excellent agreement with recent experimental results: for four bands of MgH₂ and one band of MgD₂ the root-mean-square (rms) band origin discrepancies were only 0.44 and 0.06 cm⁻¹, respectively, and the rms relative discrepancies in the inertial rotational constants ($B_{[v]}$) were only 0.0196% and 0.0058%, respectively. Spectroscopic constants for MgHD were predicted using the same potential surface.

I. Introduction

Recent years have seen a number of experimental and theoretical studies of the reaction dynamics for conversion of Mg to its hydride MgH₂.^{1–10} The ground state reaction Mg(¹S₀) + H₂(g) → MgH₂ is endoergic and is inhibited by a large barrier.^{10–12} It is generally accepted that MgH₂ is an intermediate in the gas-phase reactions Mg(¹S₀ or ¹P₁) + H₂ → MgH + H.^{1–10} However, despite its detection by infrared spectroscopy in low-temperature rare-gas matrixes,^{13,14} stable gaseous MgH₂ was not observed until the work of Shayesteh et al. in 2003.¹⁵ Their high-resolution Fourier transform infrared emission spectroscopy studies yielded band origins and rotational constants for four vibrational bands of MgH₂ and one of MgD₂.^{15,16}

Most previous theoretical studies had focused on the total electronic energy, the equilibrium geometry, and the harmonic vibrations of the MgH₂ molecule.^{11,12,17–19} Our previous work reported rotationless anharmonic vibrational energy levels on a ground-state potential energy surface (PES).²⁰ However, the discrepancies from experiment for the antisymmetric-stretch fundamental vibrational frequency and first overtone on that surface are 13.12 and 27.43 cm⁻¹ (or 0.83 and 0.87%), respectively.²¹ A recent variational configuration interaction calculation of Hrenar et al.²² using a potential energy surface calculated in a multilevel scheme (1D, CCSD(T); 2D, MP4 (SDQ); 3D, MP2) with a cc-pCVTZ basis set yielded an asymmetric stretch energy discrepancy of only 2.1 cm⁻¹ (or 0.13%) but did not report higher vibration energy levels or estimate the rotational constants. The object of the present work was therefore to calculate an accurate potential energy surface for MgH₂ and to perform accurate direct calculations of the vibration–rotation level energies to permit comprehensive comparisons with experiment for all available spectroscopic parameters.

In the following, section II describes how our new *ab initio* potential function values were calculated and how eigenvalues

on that potential energy surface were computed. Section III then presents the resulting potential energy surface, the calculated vibrational energies and vibrational and rotational constants, and compares them with experiment. Our conclusions are summarized in section IV.

II. Computational Methods

A. The Potential Energy Surface. The three-dimensional adiabatic potential energy surface for the electronic ground state of MgH₂ has been calculated using the MOLPRO package.²³ All of these calculations were first carried out using the internally contracted multireference interaction method with Davidson corrections (icMRCI+Q).²⁴ To check the basis-set convergence, we calculated the energy at every point of the PES with several versions of the augmented correlation-consistent polarized n - ζ (aug-cc-pVnZ or AVnZ) basis set.²⁵ The complete basis set (CBS) limit for valence electrons was estimated by fitting the energies $E_{\text{AVnZ}}^{\text{valence}}$ from a series of AVnZ results to the exponential function of van Mourik and co-workers, $E_{\text{CBS}}^{\text{valence}} = E_{\text{AVnZ}}^{\text{valence}} + Ae^{-n} + Be^{-n^2}$ (with $n = 3, 4,$ and 5 corresponding to AVTZ, AVQZ, and AV5Z, respectively). The employment of an augmented correlation-consistent polarized n - ζ basis set resulted in a total of 96 cGTOs (contracted Gaussian-type orbitals) for AVTZ, 176 cGTOs for AVQZ, and 291 cGTOs for AV5Z, respectively. All reference states were taken from the natural orbitals for a state-averaged complete active space self-consistent-field (CASSCF) calculation for equally weighted $1^1A'$, $2^1A'$, and $1^1A''$ states. Four active electrons and six active orbitals were used, including one for each of the hydrogens and four for Mg. The five core orbitals of Mg were fully optimized, while being constrained to be doubly occupied and excluded from the fully valence active space, denoted MCSCF(4,6), where MCSCF means multiconfiguration self-consistent field. In the subsequent multireference configuration interaction (MRCI) calculations, the reference functions were taken to be the same as those in the CASSCF active space. The total number of contracted configurations in the MRCI calculations was about

* To whom correspondence should be addressed. E-mail: huili@uwaterloo.ca.

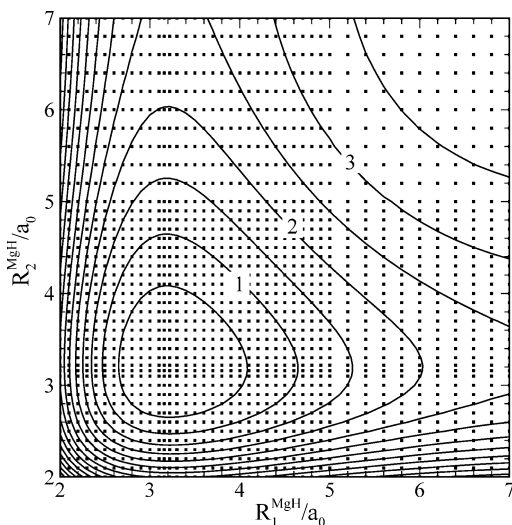


Figure 1. Grid placement and contour plots in internal coordinates for MgH₂ at $\gamma = 180^\circ$. Contours are separated by 0.5 eV, with the zero of energy set at the potential minimum.

0.73×10^6 for AV5Z. All calculations were performed in the C_s symmetry framework.

To determine the core-electron correlation contribution, which is defined as the difference between the energies of a valence-only and core-plus-valence electron calculation, the energies were calculated at every point on the potential energy surface using the averaged coupled-pair functional (ACPF) method.²⁶ This was done both because it is desirable to use a size-extensive method when a large numbers of electrons are correlated and because it is preferred to use a multireference method when describing a bond breaking process. The core-electron correlation energies were calculated employing a series of correlation-consistent polarized core-valence $n-\zeta$ basis sets²⁵ (cc-pCVnZ or CVnZ for $n = 3, 4,$ and 5) and extrapolated to the complete basis set limit using the extrapolation method described above. Thus, all potential energy values were expressed as

$$E_{ACVnZ}^{\{\text{valence}+\text{core}\}} = E_{AVnZ}^{\{\text{valence}\}} + [E_{CVnZ}^{\{\text{valence}+\text{core}\}} - E_{CVnZ}^{\{\text{valence}\}}] \quad (1)$$

For compactness, in the rest of the present paper calculations performed without and with the core-electron correlation contributions are called AVnZ and ACVnZ, respectively, where $n = 3, 4,$ and 5 for different ζ values, and the CBS limit for valence-only and all-electron correlation are labeled CBS(V) and CBS(V+C), respectively. Our optimum potential energy surface is CBS(V+C).

A nonuniform direct-product grid in the internal coordinate system was selected for calculation of the potential energy surface. In order to obtain a particularly accurate surface, we chose a relatively dense grid in the Mg–H stretching coordinates consisting of 42 points ranging from 2.0 to 7.0 a_0 . The bending coordinate was sampled at 10 values of the enclosed angle, ranging from 90 to 180°. The distribution and density of these points are illustrated in Figures 1 and 2. This gives a total of 9030 symmetry-unique points. Three-dimensional spline interpolation was used to provide values of the potential at configurations between the grid points. The potential contours and the interpolation techniques are discussed below. In some configurations where orbital mixing is strong, the MRCI and ACPF calculations experienced convergence difficulties. In those situations, we used the converged natural orbitals of a nearby geometry as the initial guess to improve the convergence.

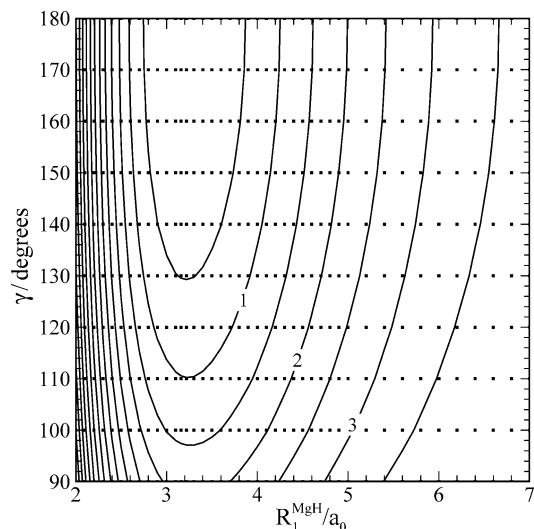


Figure 2. Grid placement and contour plots in internal coordinates for MgH₂ at $R_2^{\text{MgH}} = 3.22 a_0$. Contours are separated by 0.5 eV, with the zero of energy set at the potential minimum.

To study the barrier for the reaction involving insertion of Mg into H₂ on a reaction path with C_{2v} symmetry, 46 energy points in the vicinity of the transition state were calculated at the same level of theory as before using Jacobi coordinates ($R, r = r_{\text{HH}}, \chi$), in which R is the distance between the Mg atom and the center of the H–H bond, and the angle between \vec{R} and the H–H bond axis is fixed at $\chi = 90^\circ$. Near the maximum on that path, the potential can be written as the double polynomial expansion:

$$V(r, R) = V_0 + c_{1,0}r + c_{0,1}R + c_{2,0}r^2 + c_{0,2}R^2 + c_{1,1}rR \quad (2)$$

Expansion coefficients determined from a least-squares fit to those 46 points were used to determine the geometry parameters and energy of the transition state.

B. Calculation of Energy Levels and Spectroscopic Constants. Within the Born–Oppenheimer approximation, the rovibrational Hamiltonian of a triatomic molecule in the Radau coordinate system (R_1, R_2, θ) with the total angular momentum representation in the body-fixed reference frame can be written as (in atomic units)^{27–29}

$$\hat{H} = -\frac{1}{2m_1} \frac{\partial^2}{\partial R_1^2} - \frac{1}{2m_2} \frac{\partial^2}{\partial R_2^2} + \left(\frac{1}{2m_1 R_1^2} + \frac{1}{2m_2 R_2^2} \right) \left(\frac{-1}{\sin \theta} \frac{\partial}{\partial \theta} \sin \theta \frac{\partial}{\partial \theta} + \frac{\hat{J}_z^2}{\sin^2 \theta} \right) + \frac{\hat{J}^2 - 2\hat{J}_z^2}{2m_1 R_1^2} + \frac{\cot \theta}{2m_1 R_1^2} [\hat{J}_x + i\hat{J}_y) + (\hat{J}_x - i\hat{J}_y)] \hat{J}_z + \frac{1}{2m_1 R_1^2} \frac{\partial}{\partial \theta} [(\hat{J}_x + i\hat{J}_y) - (\hat{J}_x - i\hat{J}_y)] + V(R_1, R_2, \theta) \quad (3)$$

in which m_1 and m_2 are the masses of the two H atoms. The transformation between Radau coordinates (R_1, R_2, θ) and the conventional bond-length/bond-angle coordinates ($R_1^{\text{MgH}}, R_2^{\text{MgH}}, \gamma$) is well documented.²⁷ Because of the mass disparity between H and Mg, the radial Radau coordinates R_1 and R_2 are close to but not identical with the corresponding molecular Mg–H bonds R_1^{MgH} and R_2^{MgH} . The operators $\hat{J}_x, \hat{J}_y,$ and \hat{J}_z are the components of the total angular momentum operator in the body-fixed frame. The z axis of the body-fixed frame lies along the R_1 radial Radau vector. The above Hamiltonian contains full vibration–rotation coupling.

TABLE 1: Geometric Parameters and Total Energies for the Equilibrium Geometry and Transition State of Ground-State MgH₂ Calculated with Various Basis Sets

correlation	levels	ref	equilibrium		transition state to Mg + H ₂		
			<i>r</i> (MgH) (<i>a</i> ₀)	energy + 200 (hartree)	<i>r</i> (MgH) (<i>a</i> ₀)	angle γ (deg)	energy + 200 (hartree)
valence	CCSD(T)/cc-pVQZ	18	3.2326	−0.815 801			
	CCSDT/cc-pVQZ	18	3.2329	−0.815 943			
	CISDTQ/cc-pVQZ	18	3.2329	−0.815 960			
	MRCI/CBS(V)	20	3.2306	−0.818 686	3.431	53.88	−0.705 660
valence and core	CBS(V)	present	3.2306	−0.818 768	3.4672	53.92	−0.705 290
	ACVTZ	present	3.2196	−1.116 572	3.4554	54.13	−1.003 325
	ACVQZ	present	3.2119	−1.170 259	3.4428	53.99	−1.056 793
	ACV5Z	present	3.2072	−1.193 828	3.4374	53.82	−1.080 083
	CBS(V+C)	present	3.2045	−1.207 553	3.4342	53.72	−1.093 642

A direct-product discrete variable representation (DVR) grid³⁰ was used in the rovibrational energy level calculation. Each stretching coordinate was represented by a 70-point potential-optimized DVR grid derived from the one-dimensional Hamiltonian, in which two other coordinates were fixed at their equilibrium values, with a 200 equidistant-point sine-DVR grid on the interval [2.2, 5.5] *a*₀. Some 60 Gauss–Legendre grid points on the interval [90–180°] were used for the angular variable. In addition, the potential cutoff was placed at 5.0 eV. The Lanczos algorithm was used to calculate the rovibrational energy levels for *J* = 0–8 by recursively diagonalizing the discretized Hamiltonian matrix. Ten thousand Lanczos iterations were found adequate to converge the energies of levels lying within 8000 cm^{−1} of the potential minimum to better than 0.001 cm^{−1}. Spurious eigenvalues were removed using the method detailed in ref 31. When eigenfunctions were needed, the Lanczos recursion was repeated to assemble the wave functions of interest.³²

To determine spectroscopic constants for MgH₂, MgD₂, and MgHD, a least-squares fit was performed to the rotational sublevels for each vibrational level. The total energy of a linear triatomic molecule in its ground electronic state can be separated into vibrational and rotational parts:

$$E_{\text{vib-rot}} = G(v_1, v_2^l, v_3) + F_{[v]}(J) \quad (4)$$

The vibrational energy $G(v_1, v_2^l, v_3)$, including first-order harmonic and second-order anharmonic terms, can be written as³³

$$G(v_1, v_2^l, v_3) = \omega_1 \left(v_1 + \frac{1}{2} \right) + \omega_2 (v_2 + 1) + \omega_3 \left(v_3 + \frac{1}{2} \right) + x_{11} \left(v_1 + \frac{1}{2} \right)^2 + x_{22} (v_2 + 1)^2 + x_{33} \left(v_3 + \frac{1}{2} \right)^2 + x_{12} \left(v_1 + \frac{1}{2} \right) (v_2 + 1) + x_{13} \left(v_1 + \frac{1}{2} \right) \left(v_3 + \frac{1}{2} \right) + x_{23} (v_2 + 1) \left(v_3 + \frac{1}{2} \right) + g_{22} l^2 \quad (5)$$

and the rotational energy levels can be expressed as³⁴

$$F_{[v]}(J) = B_{[v]}[J(J+1) - l^2] - D_{[v]}[J(J+1) - l^2]^2 + \frac{1}{2}(q_{[v]}J(J+1) + q_{[v]}^D[J(J+1)]^2) \quad (6)$$

$$F_{[v]}(J) = B_{[v]}[J(J+1) - l^2] - D_{[v]}[J(J+1) - l^2]^2 - \frac{1}{2}(q_{[v]}J(J+1) + q_{[v]}^D[J(J+1)]^2) \quad (7)$$

in which $G(v_1, v_2^l, v_3)$ is the pure vibrational energy for level $[v] = (v_1, v_2^l, v_3)$ expressed relative to the zero-point level at $G(0, 0^0, 0)$, v_1 , v_2 , and v_3 are the vibrational quantum numbers

for the symmetric stretching, bending, and antisymmetric stretching modes, respectively, and *l* is the vibrational angular momentum quantum number (*l* = 0, 1, and 2 for Σ , Π , and Δ levels, respectively). As usual, $B_{[v]}$ is the inertial rotational constant, $D_{[v]}$ the leading centrifugal distortion constant associated with a given vibrational level, and *J* is the total angular momentum quantum number (including internal rotation). For Σ states, the constants $q_{[v]} = q_{[v]}^D = 0$, but these coefficients are nonzero for the Π and Δ states, and eqs 6 and 7 refer to the $e(+)$ and $f(-)$ parity levels, respectively. For Δ states, the *l*-type rotational resonances between their $\Delta(e)$ levels and those of the associated nearby $\Sigma(e)$ states means that a 2×2 Hamiltonian matrix must be used to describe their levels.^{16,33} The rotational *l*-type resonances in MgH₂ and MgD₂ are discussed in ref 16.

The equilibrium rotational constant B_e , the vibration–rotation interaction constants α_1 , α_2 , and α_3 , and the equilibrium bond lengths r_e are determined using the usual expressions:³³

$$B_{[v]} = B_e - \alpha_1 \left(v_3 + \frac{1}{2} \right) - \alpha_2 (v_3 + 1) - \alpha_3 \left(v_3 + \frac{1}{2} \right) \quad (8)$$

$$r_e = \sqrt{\frac{\hbar^2}{4B_e m_{\text{H(D)}}}} \quad (9)$$

where m_{H} and m_{D} are the atomic masses for hydrogen and deuterium, respectively.

III. Results and Discussion

A. Potential Energy Surface. Figures 1 and 2 present contour plots of our potential energy surface for ground-state MgH₂ in internal coordinates (R_1^{MgH} , R_2^{MgH} , γ), the former showing the dependence of the potential energy surface on the two bond lengths with the interbond angle fixed at 180°, while the latter depicts its dependence on one Mg–H bond length and the bending angle while the other Mg–H bond is fixed near its equilibrium value, at 3.22 *a*₀. The overall minimum clearly lies at the linear geometry and, for our highest-level CBS(V+C) calculations, corresponds to $R_1^{\text{MgH}} = R_2^{\text{MgH}} = R_2^{\text{Mg}} = 3.2045 a_0$ (1.6957 Å). These results are compared with those obtained using several other basis sets in Table 1. It is clear that the inclusion of core correlation has a significant effect on both the equilibrium MgH bond length and the total energy. Furthermore, with the enlargement of the basis set from ACVTZ to ACV5Z and extrapolation to the estimated CBS(V+C) limit, the equilibrium bond length and total energy tend to converge to well-defined asymptotic limits.

The linear-geometry potential minimum on our surface lies 4.5424 eV (or 104.75 kcal/mol) below the asymptote corresponding to H + Mg + H, which is slightly lower than the previous theoretical estimate of 4.62 eV (106.54 kcal mol^{−1}) for this limit.²⁰ Taking account of the zero-point energy yields

TABLE 2: Calculated Energies (in eV) on the Ground-State MgH₂ Potential Energy Surface Obtained Using Various Basis Sets, Expressed Relative to the Energy at the Equilibrium Linear Geometry

correlation	basis set	transition state to Mg + H ₂	asymptote		
			Mg + H ₂	MgH + H	H + Mg + H
valence	CBS(V)	3.0879	-0.1514	3.1786	4.6218
valence and core	ACVTZ	3.0816	-0.1987	3.1394	4.5085
	ACVQZ	3.0876	-0.1964	3.1479	4.5282
	ACV5Z	3.0952	-0.1920	3.1543	4.5371
	CBS(V+C)	3.0997	-0.1893	3.1580	4.5424

TABLE 3: Root-Mean-Square Discrepancy (in cm⁻¹) on Interpolating for Omitted Potential Function Values in the Specified Energy Range, When the Independent Variable Interpolated over Was (R_i^{MgH})ⁿV for n = 0, 2, and 4

range	no. points	n = 0	n = 2	n = 4
all energies	9030	14.44	8.76	10.07
energies ≤ 20 000 cm ⁻¹	3623	0.51	0.41	0.43

an atomization energy of $D_0 = 4.2890$ eV (or 98.91 kcal/mol). To determine the location and total energy of the transition state for the reaction $\text{MgH}_2 \rightarrow \text{Mg} + \text{H}_2$, a least-squares fit was performed to 46 ab initio points located near the barrier. The resulting geometrical parameters and total energies are also given in Table 1. The saddle point of the barrier is found to lie at $R_1^{\text{MgH}} = R_2^{\text{MgH}} = 3.4342 a_0$ (1.8173 Å) and $\gamma = 53.72^\circ$, which is slightly different from our previous estimates of $R_1^{\text{MgH}} = R_2^{\text{MgH}} = 3.431 a_0$ (1.816 Å) and $\gamma = 53.9^\circ$.²⁰ This decomposition reaction is slightly exothermic by 0.1514 eV (or 3.49 kcal/mol) at the CBS(V) level and by 0.1893 eV (or 4.37 kcal/mol) at the CBS(V+C) theory of level, values which are in reasonably good agreement with the early theoretical values of 5 kcal/mol from Pople et al.¹¹ and 3 kcal/mol by Ahlrichs et al.,¹² and somewhat smaller than a more recent estimate of 0.51 eV (11.8 kcal/mol) reported by Ou and co-workers.³⁶

The other MgH₂ decomposition channel, namely, $\text{MgH}_2 \rightarrow \text{MgH} + \text{H}$, is predicted to be strongly endothermic by 3.1786 eV (73.30 kcal/mol) and 3.1580 eV (72.83 kcal/mol) at the CBS(V) and CBS(V+C) levels of theory, respectively, with no barrier on the reaction path. The calculated relative energies of various dissociation limits and of the transition state (relative to the triatomic potential minimum) at different levels of theory are summarized in Table 2. It is clear from this table that the ACV5Z energy at every stationary point is close to its CBS(V+C) counterpart, indicating excellent convergence of the geometry with respect to the size of the basis set.

B. Effect of Interpolation on the Potential Energy Surface.

Conventional “rectangular” three-dimensional spline interpolation was used to define our overall potential energy surface. The magnitude of the error introduced by the scheme used for interpolating between the grid points was estimated using the approach described in ref 37. One-by-one, each known potential function value was omitted from the grid, a chosen interpolation scheme used to estimate its value, and the resulting discrepancies averaged to provide an estimate of the amplitude of the “interpolation noise” for that particular scheme. The schemes considered performed interpolation along the bond-stretch axes while treating $(R_i^{\text{MgH}})^n V$ as the dependent variable, where the power $n = 0, 2, \text{ or } 4$; after such an interpolation is performed, division of the result by $(R_i^{\text{MgH}})^n$ yields the desired function value (see ref 37).

The first row of Table 3 shows that when all of our potential function points are considered, the root-mean-square (rms) interpolation discrepancy is reduced by almost a factor of 2 if the interpolation is performed over $(R_i^{\text{MgH}})^2 V$ rather than over the potential function itself (the case $n = 0$). This is due to the

TABLE 4: Calculated Energies (in cm⁻¹) of the 44 Lowest Pure Vibrational Levels of MgH₂, MgD₂, and MgHD on the New CBS(V+C) Potential Energy Surface (“new”) Compared with Previous Theoretical Results of Reference 37 (“diff” = “old” – “new”)a

(v_1, v_2', v_3)	MgH ₂		MgD ₂		MgHD new
	new	diff	new	diff	
(0,0 ⁰ ,0)	0.00	0.00	0.00	0.00	0.00
(0,2 ⁰ ,0)	870.63	3.15	639.77	2.33	763.75
(1,0 ⁰ ,0)	1567.47	15.05	1119.35	10.97	1578.49
(0,0 ⁰ ,1)	1588.73 ^b	13.18	1176.45 ^c	9.92	1147.54*
(0,4 ⁰ ,0)	1746.70	7.03	1281.50	5.03	1530.98*
(1,2 ⁰ ,0)	2430.77	17.54	1756.63	12.89	2331.86
(0,2 ⁰ ,1)	2446.66	15.49	1808.44	11.64	1906.33*
(0,6 ⁰ ,0)	2628.74	11.69	1925.58	8.04	2302.16*
(2,0 ⁰ ,0)	3101.79	28.66	2226.06	21.59	3111.32
(1,0 ⁰ ,1)	3110.78	27.17	2272.56	20.25	2726.73*
(0,0 ⁰ ,2)	3165.65 ^d	27.66	2341.62	20.04	2271.25*
(1,4 ⁰ ,0)	3299.46	21.06	2395.86	15.38	3088.87*
(0,4 ⁰ ,1)	3310.28	18.99	2442.62	14.00	2668.68*
(0,8 ⁰ ,0)	3516.77	16.86	2572.23	11.51	3077.38*
(2,2 ⁰ ,0)	3955.55	30.24	2860.63	23.06	3854.21
(1,2 ⁰ ,1)	3961.15	28.84	2901.97	21.55	3475.27*
(0,2 ⁰ ,2)	4013.13	29.49	2966.11	21.24	3024.98*
(1,6 ⁰ ,0)	4173.76	25.40	3037.30	18.21	3849.62*
(0,6 ⁰ ,1)	4179.82	23.45	3079.25	16.83	3434.90*
(0,10 ⁰ ,0)	4410.93	22.78	3221.42	15.17	3856.75
(3,0 ⁰ ,0)	4592.35	40.74	3319.23	31.82	4599.03
(2,0 ⁰ ,1)	4594.51	40.13	3354.07	30.26	4260.04*
(1,0 ⁰ ,2)	4674.52	43.07	3418.28	30.23	3851.12*
(0,0 ⁰ ,3)	4714.93	40.99	3494.86	30.20	3371.28*
(2,4 ⁰ ,0)	4814.11	33.17	3497.11	25.30	4600.79*
(1,4 ⁰ ,1)	4817.14	32.04	3533.56	23.74	4227.49*
(0,4 ⁰ ,2)	4867.00	32.93	3593.01	23.33	3782.35*
(1,8 ⁰ ,0)	5053.68	30.25	3681.10	21.53	4614.36
(0,8 ⁰ ,1)	5055.16	28.47	3718.46	20.15	4205.02*
(0,12 ⁰ ,0)	5311.21	29.56	3873.24	19.15	4640.30
(3,2 ⁰ ,0)	5434.56	41.58	3950.69	32.82	5331.21
(2,2 ⁰ ,1)	5435.65	41.11	3980.53	31.13	4998.22*
(1,2 ⁰ ,2)	5518.07	44.40	4040.56	31.10	4594.72*
(0,2 ⁰ ,3)	5549.47	42.00	4111.96	30.92	4119.84*
(2,6 ⁰ ,0)	5677.35	37.03	4135.62	27.96	5351.08
(1,6 ⁰ ,1)	5678.65	36.20	4167.43	26.39	4983.48*
(0,6 ⁰ ,2)	5727.22	37.36	4222.47	26.02	4543.48*
(0,10 ⁰ ,1)	5936.40	34.27	4360.20	23.71	4979.00*
(1,10 ⁰ ,0)	5939.38	35.82	4327.26*	25.05	5382.88
(4,0 ⁰ ,0)	6035.39	51.80	4397.08	41.50	6042.18
(3,0 ⁰ ,1)	6035.76	51.66	4419.71	39.91	5747.95
(2,0 ⁰ ,2)	6160.61	57.18	4481.92	40.43	5384.94*
(1,0 ⁰ ,3)	6183.30	54.95	4553.01	40.22	4951.80*
(0,14 ⁰ ,0)	6216.78	25.60	4527.87*	23.59	5427.98*
(0,0 ⁰ ,4)	6246.11	66.09	4636.10	40.39	4447.79*
(3,4,0)			4583.92*		6067.19*
(2,4,1)			4609.11*		5740.06*

^a The MgH₂ levels are listed in order of increasing energy. Level energies for the heavier isotopologues which do not appear in order of increasing energy are labeled by an asterisk, and the highest-energy level for each is shown in bold font. ^b Experimental value: 1588.67 cm⁻¹.¹⁵ ^c Experimental value: 1176.50 cm⁻¹.⁴⁰ ^d Experimental value: 3165.42 cm⁻¹.¹⁵

fact that in the steep short-range repulsive wall region, the rapid decrease of the factor $(R_i^{\text{MgH}})^2$ with decreasing bond length damps the growth of the ordinate variable, which improves the

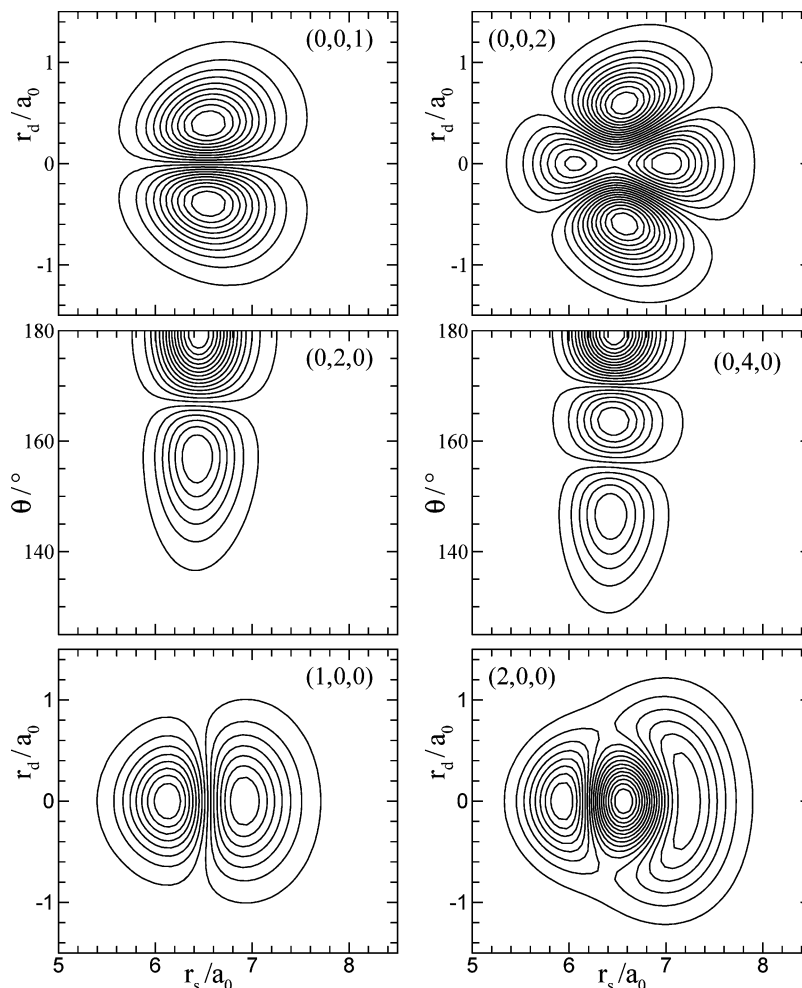


Figure 3. Contour plots for six vibrational eigenfunctions of MgH_2 : $(v_1, v_2, v_3) = (1,0,0)$, $(2,0,0)$, $(0,2,0)$, $(0,4,0)$, $(0,0,1)$, and $(0,0,2)$ plotted with respect to the sum $r_s = (R_1 + R_2)$, difference $r_d = (R_1 - R_2)$, and enclosed angle θ , of Radau coordinates.

reliability of the cubic spline interpolation procedure there.^{38,39} The fact that increasing the power further to $n = 4$ causes the rms discrepancy to increase slightly probably reflects the fact that the lower part of the outer attractive wall of our potential function is also very steep, and this further modification makes the ordinate variable there grow sufficiently rapidly with distance that a cubic spline function no longer interpolates optimally. The last row of Table 3 shows the analogous rms discrepancies for the 3623 configurations corresponding to energies within $20\,000\text{ cm}^{-1}$ of the potential minimum. Again, “ $n = 2$ interpolation” has substantially smaller discrepancies than do the other methods, and for $n = 2$, “interpolation noise” errors in the potential energy function are on average less than 1 cm^{-1} . This $n = 2$ cubic spline interpolation scheme was therefore used in our final calculations of the spectroscopic properties of MgH_2 , MgD_2 , and MgHD .

C. Vibration–Rotation Energy Levels and Spectroscopic Constants. The vibrational zero-point levels of MgH_2 , MgD_2 , and MgHD are found to lie 2044.00 (or 0.2534 eV), 1481.51 (or 0.1837 eV), and 1767.18 cm^{-1} (or 0.2191 eV), respectively, above the triatomic potential minimum. Although these zero-point levels lie far above the exoergic dissociation asymptote to yield $\text{Mg} + \text{H}_2$ (-0.1893 eV), they lie far below both the 3.0997 eV barrier on this reaction path and the dissociation asymptotes to yield $\text{MgH} + \text{H}$ (at 3.1580 eV) or $\text{H} + \text{Mg} + \text{H}$ (4.5424 eV at the CBS(V+C) level). Thus, the vibrational ground state and the low-lying excited vibrational states of this species are very stable.

TABLE 5: Vibrational Constants for Isotopic MgH_2 Determined by Fitting Eigenvalues of the CBS(V+C) Potential Surface to Eq 5, All in cm^{-1} ^a

	MgH_2	MgD_2	MgHD
ν_1	1567.47	1119.35	1578.49
ν_2	435.57 ^b	320.27	382.45
ν_3	1588.73 ^c	1176.45 ^d	1147.54
ω_1	1627.07(141)	1144.78(148)	1628.87(100)
ω_2	437.43(38)	321.28(40)	383.72(19)
ω_3	1629.50(141)	1202.96(148)	1173.47(60)
x_{11}	-16.6(4)	-6.3(4)	-22.8(3)
x_{22}	0.71(3)	0.27(4)	0.476(13)
x_{33}	-5.9(4) ^e	-5.6(4)	-11.9(1)
x_{12}	-3.69(15)	-1.25(16)	-5.16(11)
x_{13}	-45.4(6)	-23.2(6)	0.7(4)
x_{23}	-6.3(2) ^f	-3.8(2)	-2.48(6)

^a Quantities in parentheses are 95% confidence limit uncertainties in the last digits shown. ^b Compare to experimental estimate (obtained indirectly): 437 cm^{-1} .¹⁵ ^c Compare to experimental value: 1588.671 cm^{-1} .¹⁵ ^d Compare to experimental value: 1176.50 cm^{-1} .⁴⁰ ^e Compare to experimental value: 5.961 cm^{-1} .¹⁵ ^f Compare to experimental value: 5.976 cm^{-1} .¹⁵

Table 4 lists the pure vibrational ($J = 0$) level energies of MgH_2 , MgD_2 , and MgHD calculated from the CBS(V+C) potential energy surface and compares them with the previous theoretical results for MgH_2 and MgD_2 .²⁰ The first 44 levels of MgH_2 are listed in order of increasing energy, while corresponding levels of MgD_2 and MgHD which do not appear in order of increasing energy are labeled with an asterisk. The

TABLE 6: Spectroscopic Band Constants for MgH₂ (All in cm⁻¹) Determined from Our CBS(V+C) Potential Energy Surface and Their Differences (“diff” = calcd – obsd) from Available Experimental Values^{16,a}

levels	$G_v - \text{ZPE}$		$B_{[v]}$		$10^5 D_{[v]}$		$10^2 q_{[v]}$		$10^6 q_{[v]}^D$	
	calcd	diff	calcd	diff	calcd	diff	calcd	diff	calcd	diff
(0,0 ⁰ ,0)	0.00		2.8833	0.0007	3.906	-0.012				
(0,0 ⁰ ,1)	1588.73	0.06	2.8492	0.0005	3.877	-0.014				
(0,0 ⁰ ,2)	3165.65	0.23	2.8155	0.0004	3.849	-0.017				
(0,0 ⁰ ,3)	4714.93		2.7819		3.823					
(1,0 ⁰ ,0)	1567.47		2.8486		3.884					
(1,0 ⁰ ,1)	3110.78		2.8140		3.862					
(0,1 ¹ ,0)	<i>a</i>		2.8921	0.0005	4.080	-0.006	-5.0585	-0.012	3.50	0.26
(0,1 ¹ ,1)	<i>a</i> + 1582.26	-0.44	2.8579	0.0004	4.052	-0.006	-5.0117	-0.014	3.48	0.27
(0,1 ¹ ,2)	3589.37		2.8240		4.022		-4.9556		3.44	
(1,1 ¹ ,0)	1999.32		2.8571		4.055		-4.9853		3.44	
(1,1 ¹ ,1)	3536.04		2.8224		4.033		-4.9380		3.42	
(0,2 ⁰ ,0)	870.63		2.9012	0.0006	4.271	0.037				
(0,2 ² ,0)	<i>b</i>		2.9005	0.0008	4.253	0.078	-5.0922	-0.021	3.58	0.43
(0,2 ⁰ ,1)	2446.66		2.8670	0.0005	4.243	0.033				
(0,2 ² ,1)	<i>b</i> + 1575.86	-0.72	2.8662	0.0006	4.224	0.071	-5.0431	-0.023	3.56	0.51
(0,2 ⁰ ,2)	4013.13		2.8329		4.210					
(0,2 ² ,2)	4016.26		2.8321		4.192		-4.9846		3.51	

^a *a* = 435.57 cm⁻¹. *b* = 874.06 cm⁻¹.

TABLE 7: Spectroscopic Band Constants for MgD₂ (All in cm⁻¹) Determined from Our CBS(V+C) Potential Energy Surface

	$G_{[v]} - \text{ZPE}$	$B_{[v]}$	$10^5 D_{[v]}$	$10^2 q_{[v]}$	$10^7 q_{[v]}^D$
(0,0 ⁰ ,0)	0.00	1.446 53 ^a	0.9699 ^b		
(0,0 ⁰ ,1)	1176.45 ^c	1.433 12 ^d	0.9624 ^e		
(0,0 ⁰ ,2)	2341.62	1.419 86	0.9550		
(0,0 ⁰ ,3)	3494.86	1.406 69	0.9478		
(1,0 ⁰ ,0)	1119.35	1.434 29	0.9657		
(1,0 ⁰ ,1)	2272.56	1.420 74	0.9590		
(0,1 ¹ ,0)	320.27	1.450 44	1.0041	-1.7267	5.969
(0,1 ¹ ,1)	1492.75	1.437 00	0.9967	-1.7216	5.964
(0,1 ¹ ,2)	2654.11	1.423 71	0.9892	-1.7160	5.949
(1,1 ¹ ,0)	1438.35	1.438 12	0.9993	-1.7016	5.861
(1,1 ¹ ,1)	2587.55	1.424 54	0.9926	-1.6959	5.854
(0,2 ⁰ ,0)	639.77	1.454 45	1.0402		
(0,2 ⁰ ,1)	642.07	1.454 24	1.0380	-1.7366	6.094
(0,2 ⁰ ,2)	1808.44	1.440 99	1.0329		
(0,2 ² ,1)	1810.65	1.440 78	1.0306	-1.7309	6.071
(0,2 ⁰ ,2)	2966.11	1.427 67	1.0255		
(0,2 ² ,2)	2968.24	1.427 46	1.0232	-1.7248	6.069

^a Difference (calcd – obsd) with experimental value: -0.000 04 cm^{-1.40} ^b Difference (calcd – obsd) with experimental value: 0.011 cm^{-1.40} ^c Difference (calcd – obsd) with experimental value: -0.06 cm^{-1.40} ^d Difference (calcd – obsd) with experimental value: -0.000 11 cm^{-1.40} ^e Difference (calcd – obsd) with experimental value: 0.010 cm^{-1.40}

highest level energy for each isotopologue in this range is shown in bold font, and the two additional levels of MgD₂ lying below that highest level are included at the end of the list. For MgHD, an additional nine levels lying below the bold-font level (4, 0⁰, 0) are not listed. For MgH₂ and MgD₂, the quantum numbers (ν_1, ν_2, ν_3) represent the symmetric stretch, bend, and antisymmetric stretch modes, respectively, while for MgHD they represent the Mg–H stretch, the H–Mg–D bend, and the Mg–D stretch modes, respectively. For MgH₂, our calculated fundamental frequency for the antisymmetric-stretch vibration and its first overtone, 1588.73 and 3165.65 cm⁻¹, are in very good agreement with the experimental gas-phase values of Shayesteh et al.¹⁵ 1588.67 and 3165.42 cm⁻¹, respectively. Similarly, our value for the fundamental antisymmetric-stretch energy for MgD₂, 1176.45 cm⁻¹, agrees very well with the experimental gas-phase value of 1176.50 cm^{-1.40} No experimental infrared spectra for MgHD have been reported to date. The present results are clearly considerably improved relative to those of our earlier work.²⁰

TABLE 8: Spectroscopic Band Constants for MgHD (All in cm⁻¹) Calculated from Our CBS(V+C) Potential Energy Surface

level	$G_{[v]} - \text{ZPE}$	$B_{[v]}$	$10^5 D_{[v]}$	$10^2 q_{[v]}$	$10^6 q_{[v]}^D$
(0,0 ⁰ ,0)	0.00	1.9504	1.9270		
(0,0 ⁰ ,1)	1147.54	1.9285	1.8645		
(0,0 ⁰ ,2)	2271.25	1.9065	1.9286		
(0,0 ⁰ ,3)	3371.28	1.8845	1.9316		
(1,0 ⁰ ,0)	1578.49	1.9340	1.8996		
(2,0 ⁰ ,0)	3111.32	1.9176	1.9213		
(1,0 ⁰ ,1)	2726.73	1.9124	1.8990		
(1,0 ⁰ ,2)	3851.12	1.8907	1.7596		
(2,0 ⁰ ,1)	4260.04	1.8961	1.8812		
(0,1 ¹ ,0)	382.45	1.9555	1.9904	-2.6422	1.284
(0,1 ¹ ,1)	1527.47	1.9334	1.9748	-2.6099	1.242
(0,1 ¹ ,2)	2648.61	1.9113	1.9891	-2.5728	1.266
(1,1 ¹ ,0)	1955.65	1.9391	1.9640	-2.6290	1.256
(2,1 ¹ ,0)	3483.13	1.9231	2.0427	-2.5442	0.118
(1,1 ¹ ,1)	3101.44	1.9171	1.9365	-2.6366	1.756
(0,2 ⁰ ,0)	763.75	1.9609	2.0623		
(0,2 ⁰ ,1)	767.56	1.9602	2.0497	-2.6591	1.314
(1,2 ⁰ ,0)	2331.86	1.9444	2.0360		
(1,2 ⁰ ,1)	2335.46	1.9438	2.0243	-2.6457	1.280
(0,2 ⁰ ,1)	1906.33	1.9386	2.0583		
(0,2 ² ,1)	1910.10	1.9379	2.0397	-2.6259	1.304
(0,2 ⁰ ,2)	3024.98	1.9163	2.0582		
(0,2 ² ,2)	3028.72	1.9156	2.0452	-2.5884	1.294

Contour plots of the wave functions for selected vibrational levels of MgH₂ are shown in Figure 3, plotted versus the symmetric and antisymmetric combinations of Radau coordinates $r_s = R_1 + R_2$ and $r_d = R_1 - R_2$. The nodal structures of these wave functions are quite clear; wave function plots of this type were used to make the vibrational assignments for the levels listed in Table 4.

Fitting the CBS(V+C) vibrational energies of the 11 lowest levels with $l = 0$ to eq 5 yielded the vibrational constants shown in Table 5; for completeness, the fundamental vibrational spacings ν_i are listed there too. In view of the uncertainties associated with the determination of coefficients from truncated expansions, our estimates of the anharmonicity constants x_{33} and x_{23} may be considered in good agreement with experiment.

Table 6 presents a detailed comparison of our calculated band origins and rotational constants on the CBS(V+C) potential energy surface with the experimental spectroscopic constants for all of the emission bands of MgH₂ reported by Shayesteh et al.^{15,16} To facilitate direct comparisons with the experimental

TABLE 9: Comparison of Equilibrium Properties and Ground-State Rotational Constants of Our CBS(V+C) Potential Energy Surface with the Corresponding Experimental Values^{15,40}

	MgH ₂			MgD ₂		
	calcd	obsd ¹⁵	calcd – obsd	calcd	obsd ⁴⁰	calcd – obsd
B_e/cm^{-1}	2.9093(9)	2.90818(15) ^a	0.00112	1.45552(30)		
$r_e/\text{Å}$	1.69549(26)	1.69582(4) ^a	–0.00033	1.69564(17)		
B_0/cm^{-1}	2.8832965(86)	2.882607(11)	0.0006895	1.44653366(89)	1.446575(14)	–0.00004134
$r_0/\text{Å}$	1.703123(3)	1.703327(3)	–0.000204	1.7008979(5)	1.700874(8)	0.0000239
α_1/cm^{-1}	0.0351(3)			0.01234(9)		
α_2/cm^{-1}	–0.0087(3)	–0.008950(18)	0.00025	–0.00389(10)		
α_3/cm^{-1}	0.0340(3)	0.033940(15)	0.00006	0.01336(8)		

^a This experimental equilibrium structure for MgH₂ was obtained by combining our theoretical value of α_1 with the experimental values for B_0 , α_2 , and α_3 .

band origins, our calculated energies for the lower levels of vibrational transitions which are not directly connected to the ground state are shown as footnotes, rather than in the table itself. The calculated constants are clearly in very good agreement with the observed values:^{15,16} the root-mean-square discrepancies are roughly 0.0196% for the $B_{[v]}$ rotational constants and 0.95% for the $D_{[v]}$ centrifugal distortion constants, while the rms discrepancy with the four observed band origins was only 0.44 cm^{–1}. The analogous calculated band constants for MgD₂ and MgHD are shown in Tables 7 and 8. The rms discrepancies for the rotational constants of MgD₂ are only 0.0058% for $B_{[v]}$ and 1.11% $D_{[v]}$, respectively, and that for the band origins was 0.06 cm^{–1}.

Our calculated eigenvalues also allow us to generate estimates of the g_{22} constant associated with the l -dependent term in the vibrational level energy expression for a symmetric triatomic molecule. For Π ($l = 2$) and Σ ($l = 0$) vibrational levels,¹⁶

$$g_{22} = \frac{[G(v_1, v_2^2, v_3) - G(v_1, v_2^0, v_3)]}{4} \quad (10)$$

The results in Tables 6 and 7 therefore yield values of $g_{22} = 0.8588, 0.8156, \text{ and } 0.7834 \text{ cm}^{-1}$ for the (0,2,0), (0,2,1), and (0,2,2) levels of MgH₂ and $g_{22} = 0.5760, 0.5533, \text{ and } 0.5331 \text{ cm}^{-1}$ for the (0,2,0), (0,2,1), and (0,2,2) levels of MgD₂. These are within 0.06 cm^{–1} of the experimental values of Shayesteh et al.¹⁶

Finally, the calculated inertial rotational constants $B_{[v]}$ for the 18 lowest vibrational levels of MgH₂ and MgD₂ were fitted to eq 8 to determine the equilibrium constants B_e and the anharmonicity constants α_i . These constants, together with the associated equilibrium and zero-point level bond lengths, are listed in Table 9, where they are compared with the best available experimental values of these quantities. As seen there, although the bond lengths for isotopologues of MgH₂ and MgD₂ are slightly different, those differences are within the estimated uncertainties. Earlier ab initio calculations by Tschumper and Schaefer III¹⁸ at the CCSDT and CISDTQ level with a cc-pVQZ basis set had predicted $R_e = 1.710\,777 \text{ Å}$, which is in reasonably good agreement with our result (1.695 49 Å), the difference probably being due to their calculation not including core correlation and the relatively small basis set they used.

IV. Conclusions

We report a new ab initio potential energy surface for the ground electronic state of MgH₂ consisting of 9030 symmetry-unique points obtained at the iMRCI+Q level with extrapolation to the complete basis set limit and including the effect of core-electron correlation. Eigenvalues of low-lying levels of MgH₂, MgD₂, and HMgD calculated using the iterative Lanczos method converged to better than 0.001 cm^{–1} and were used to

generate the energies and rotational constants of a number of vibrational levels of the three isotopologues, MgH₂, MgD₂, and MgHD. These results are in excellent agreement with the gas-phase spectroscopic results of Shayesteh et al.:^{15,16,40} our band origins have rms discrepancies of only 0.44 and 0.06 cm^{–1}, while our inertial rotational constants have rms relative discrepancies with experiment of only 0.0196% and 0.0058% for MgH₂ and MgD₂, respectively. These band origin discrepancies are much smaller than those obtained in our previous ab initio treatment of this system, in which the calculations did not take account of core/valence correlation effects.²⁰ The agreement obtained here demonstrates the high quality of our potential energy surface and indicates that our predictions of the properties of unobserved levels should be quite reliable.

Acknowledgment. We are pleased to acknowledge helpful discussions with Professor P. F. Bernath and Dr. A. Shayesteh. We are also grateful to Professor K. Peterson for providing us with his new Mg atom basis set prior to publication. This research was supported by the Natural Sciences and Engineering Research Council of Canada.

Supporting Information Available: The 9030 symmetry-unique ab initio values of our recommended CBS(V+C) potential energy surface for MgH₂, a Fortran subroutine for interpolating over those points for any values of the system coordinates, a listing of the calculated rotational level energies used to generate the constants in Tables 6–8, and listings of the $J = 0–8$ level energies used to determine the rotational constants presented in Tables 5–7. This material is available free of charge via the Internet at <http://pubs.acs.org>.

References and Notes

- (1) Kleiber, P. D.; Lyyra, A. M.; Sando, K. M.; Heneghan, S. P.; Stwalley, W. C. *Phys. Rev. Lett.* **1985**, *54*, 2003.
- (2) Kleiber, P. D.; Lyyra, A. M.; Sando, K. M.; Zafirooulos, V.; Stwalley, W. C. *J. Chem. Phys.* **1986**, *85*, 5493.
- (3) Breckenridge, W. H.; Wang, J. H. *Chem. Phys. Lett.* **1987**, *137*, 195.
- (4) Breckenridge, W. H.; Umamoto, H. *J. Chem. Phys.* **1984**, *80*, 4168.
- (5) Lin, K. C.; Huang, C. T. *J. Chem. Phys.* **1989**, *91*, 5387.
- (6) Breckenridge, W. H.; Huang, J. H. *Chem. Phys. Lett.* **1987**, *139*, 28.
- (7) Breckenridge, W. H.; Stewart, J. *J. Chem. Phys.* **1982**, *77*, 4469.
- (8) Breckenridge, W. H.; Umamoto, H. *J. Chem. Phys.* **1981**, *75*, 698.
- (9) Liu, D. K.; Chin, T. L.; Lin, K. C. *Phys. Rev. A* **1994**, *50*, 4891.
- (10) Breckenridge, W. H. *J. Phys. Chem.* **1996**, *100*, 14840.
- (11) Pople, J. A.; Luke, B. T.; Frisch, M. J.; Binkley, J. S. *J. Phys. Chem.* **1985**, *89*, 2198.
- (12) Ahlrichs, R.; Keil, F.; Lischka, H.; Kutzelnigg, W.; Staemmler, V. *J. Chem. Phys.* **1975**, *63*, 455.
- (13) Tague, T. J.; Andrews, L. *J. Phys. Chem.* **1994**, *98*, 8611.
- (14) McCaffrey, J. G.; Parnis, J. M.; Ozin, G. A.; Breckenridge, W. H. *J. Phys. Chem.* **1985**, *89*, 4945.
- (15) Shayesteh, A.; Appadoo, D. R. T.; Gordon, I.; Bernath, P. F. *J. Chem. Phys.* **2003**, *119*, 7785.

- (16) Shayesteh, A.; Bernath, P. F. *J. Chem. Phys.* **2006**, *124*, 156101.
(17) von Szentpaly, L. *J. Phys. Chem. A* **2002**, *106*, 11945.
(18) Tschumper, G. S.; Schaefer, H. F., III. *J. Chem. Phys.* **1998**, *108*, 7511.
(19) Chaquin, P.; Sevin, A.; Yu, H. *J. Phys. Chem.* **1985**, *89*, 2813.
(20) Li, H.; Xie, D. Q.; Guo, H. *J. Chem. Phys.* **2004**, *121*, 4156.
(21) Shayesteh, A.; Tereszchuk, K.; Bernath, P. F. *J. Chem. Phys.* **2003**, *118*, 3622.
(22) Hrenar, T.; Werner, H.-J.; Rauhut, G. *Phys. Chem. Chem. Phys.* **2005**, *7*, 3123.
(23) Werner, H. J.; Knowles, P. J.; Amos, R. D.; Berning, A.; Cooper, D. L.; Deegan, M. J. O.; Dobbyn, A. J.; Eckert, F.; Elbert, S. T.; Hampel, C.; Lindh, R.; Lloyd, A. W.; Meyer, W.; Nicklass, A.; Peterson, K.; Pitzer, R.; Stone, A. J.; Taylor, P. R.; Mura, M. E.; Pulay, P.; Schutz, M.; Stoll, H.; Thorsteinsson, T. *MOLPRO*; a package of ab initio programs; University College Cardiff Consultants Limited: Wales, U.K.
(24) Langhoff, S. R.; Davidson, E. R. *Int. J. Quantum Chem.* **1974**, *8*, 61.
(25) Woon, D. E.; Peterson, K. A.; Dunning, T. H., Jr. Private communication, 2005.
(26) Gdanitz, R. J.; Ahlrichs, R. *Chem. Phys. Lett.* **1988**, *143*, 413.
(27) Johnson, B. R.; Reinhardt, W. P. *J. Chem. Phys.* **1986**, *85*, 4538.
(28) Choi, S. E.; Light, J. C. *J. Chem. Phys.* **1990**, *92*, 2129.
(29) Sutcliffe, B. T.; Tennyson, J. *Int. J. Quantum Chem.* **1991**, *39*, 183.
(30) Light, J. C.; Hamilton, I. P.; Lill, J. V. *J. Chem. Phys.* **1985**, *82*, 1400.
(31) Chen, R.; Guo, H. *J. Chem. Phys.* **1999**, *111*, 9944.
(32) Cullum, J. K.; Willoughby, R. A. *Lanczos Algorithms for Large Symmetric Eigenvalue Computations*; Birkhauser: Boston, MA, 1985.
(33) Bernath, P. F. *Spectra of Atoms and Molecules*, 2nd ed.; Oxford University: New York, 2005.
(34) Herzberg, G. *Molecular Spectra and Molecular Structure II. Infrared and Raman Spectra of Polyatomic Molecules*; Krieger: Malabar, FL, 1991.
(35) Papousek, D.; Aliev, M. R. *Molecular Vibrational-Rotational Spectra*; Elsevier: Amsterdam, The Netherlands, 1982.
(36) Ou, Y. R.; Liu, D. K.; Lin, K. C. *J. Chem. Phys.* **1998**, *108*, 1475.
(37) Li, H.; Le Roy, R. J. *J. Chem. Phys.* **2006**, *125*, 044307.
(38) Poll, J. D.; Karl, G. *Can. J. Phys.* **1966**, *44*, 1467.
(39) Le Roy, R. J.; Bernstein, R. B. *J. Chem. Phys.* **1968**, *49*, 4312.
(40) Shayesteh, A.; Appadoo, D. R.; Gordon, I.; Bernath, P. F. *Can. J. Chem.* **2004**, *82*, 947.